Revista Colombiana de Química
ISSN: 0120-2804
ISSN: 2357-3791
rcolquim_fcbog@unal.edu.co
Universidad Nacional de Colombia
Colombia

Structural analysis of adsorption processes of 5FU and imiquimodon hydrogels using AMBER/PM3 hybrid model

Rangel-Vázquez, Norma Aurea; Villanueva-Garcia, Dulce Nallely; Kalla, Jonathan
Structural analysis of adsorption processes of 5FU and imiquimodon hydrogels using AMBER/PM3 hybrid model
Revista Colombiana de Química, vol. 47, no. 2, 2018
Universidad Nacional de Colombia, Colombia
Available in: https://www.redalyc.org/articulo.oa?id=309055565004
DOI: https://doi.org/10.15446/rev.colomb.quim.v47n2.67352

Fisicoquímica e Inorgánica

Structural analysis of adsorption processes of 5FU and imiquimodon hydrogels using AMBER/PM3 hybrid model

Análisis estructural de los procesos de adsorción de 5FU e imiquimod en hidrogeles utilizando el modelo híbrido AMBER/PM3

Análise estrutural de procedimentos de adsorção de 5FU e imiquimod em hidrogeles usando modelo híbrido AMBER/PM3

Norma Aurea Rangel-Vázquez
Instituto Tecnológico de Aguascalientes, México
book_hydrogel@yahoo.com

Dulce Nallely Villanueva-Garcia
Instituto Tecnológico de Aguascalientes, México
dulce_nallely@yahoo.com

Jonathan Kalla
Program management Department-NVLPC, Estados Unidos
jhkalla@gmail.com

DOI: https://doi.org/10.15446/rev.colomb.quim.v47n2.67352
Redalyc: https://www.redalyc.org/articulo.oa?id=309055565004

Received: 30 August 2017
Accepted: 17 November 2017

Abstract:

AMBER/PM3 hybrid model allowed determining the structural properties of 5FU and imiquimod individually and after the adsorption in chitosan hydrogels crosslinked with genipin, respectively. It was observed that the Gibbs free energy (ΔG) decreases with the adsorption, but indicates thermodynamic stability and spontaneity in both processes; ΔG was verified by the increase in the dipole moments. On the one hand the partition coefficient established the hydrophilic character with respect to the water present in the hydrogel, which increases with the adsorption. The FTIR showed that there were displacements in the signals, however, the hydrogen bond bands attributed to the formation of new bonds to perform the adsorption of the drugs were observed. The adsorption was verified by the MESP and the surface analysis, where the distribution of nucleophilic and electrophilic zone was observed.

Keywords: 5FU, Imiquimod, AMBER, PM3, FTIR, MESP, Gibbs.

Resumen:

El modelo hibrido AMBER/PM3 permitió determinar las propiedades estructurales del 5FU e imiquimod individualmente y después de la adsorción en hidrogeles de quitosano entrecruzados con genipina, respectivamente. Se observó que la energía libre de Gibbs (ΔG) disminuye con la adsorción, sin embargo, en ambos procesos se encontró estabilidad termodinámica y espontaneidad; ΔG fue verificado mediante el incremento en los momentos dipolares. Por otro lado, el coeficiente de partición estableció el carácter hidrofilico con respecto al agua presente en el hidrogel, el cual aumenta con la adsorción. El FTIR evidenció que existen desplazamientos en las señales. Se observaron las bandas de puente de hidrógeno, atribuidas a la formación de enlaces, para realizar la adsorción de los fármacos. La adsorción fue verificada mediante los MESP y los análisis de superficie, en donde se apreció la distribución de zonas nucleofílicas y electrofílicas.

Palabras clave: 5FU, Imiquimod, AMBER, PM3, FTIR, MESP, Gibbs.

Resumo:

Author notes

book_hydrogel@yahoo.com

O modelo hibrido AMBER/PM3 permitiu determinar as propriedades estruturadas do 5FU e imiquimod individualmente e depois da adsorção em hidrogeles de quitosano entrecruzados com genipina, respectivamente. Observou-se que o poder livre de Gibbs (ΔG) diminui com a adsorção, sem embargo, em ambos os processos se encontró estabilidade termodinâmica e espontaneidad; ΔG foi verificado através do aumento nos momentos de dipolares. Por outro lado, o coeficiente de divisão estabeleceu o carácter hidrofílico em relação à água presente no hidrogel, o qual aumenta com a adsorção. El FTIR evidenció que existem deslocamentos em las señales. Se observe as bandas de puente de hidrógeno, atribuições à formação de enlaces, para realizar a adsorção dos fármacos. A adsorção foi verificada através do MESP e os análises de superfície, em donde se apreciou a distribuição de zonas nucleofílicas e eletrofílicas.

Palavras-chave: 5FU, Imiquimod, AMBER, PM3, FTIR, MESP, Gibbs.

Introduction

Nanomedicine is the science that applies nanotechnology. It is of major importance due to the early detection of diseases, making it possible to develop nanosystems for the treatment of diseases using the design of new drugs and carriers (*1 – 4*).The main applications of nanomedicine are the controlled release systems and the diagnoses of diseases as well as imaging analysis. Nanometric scale controlled delivery systems have the objective of transporting and releasing drug in a specific place obtaining a treatment of greater effectiveness (*5* , *6*). For this purpose hydrogels are used due to a greater affinity in the adsorption and release of the drug, the biocompatibility with the human body, biodegradability, the permeability, non–toxicity (*1 – 3* , *7*), and the adhesiveness of the three–dimensional structure that allows the hydrogels to be used in the processes of skin healing and cancer treatments (*8*).

In the last five years, the skin cancer treated by surgery had an 80% mortality rate. The main types of skin cancer are basal cells (BCC), squamous cells (SCC), and malignant melanoma. The drugs most often used in skin cancer therapies are 5–fluorouracil (5FU) and imiquimod.

5FU is an antimetabolite whose function is to inhibit the metabolic process of the cells generating cell death at the stage of mitosis (*9*). The antimetabolites have a structure very similar to the normal molecules of the human body (*10*).The structure consists of an organic aromatic heterocyclic with a fluorine atom in carbon 5. Due to its structure, 5FU interferes with nucleoside metabolism and can be incorporated into the RNA and DNA chains, leading to cytotoxicity and cell death. Its active form inhibits DNA synthesis by inhibiting the normal production of thymidine. It is primarily used for colon, chest, and neck cancer treatments (*11* , *12*).

5FU is used in a cream form for treatments of actinic keratosis and basal cell carcinoma; however, in an injected form it produces effects in the central nervous system.

The effectiveness is attributed to the irreversible union with the enzyme thymidylate synthase, essential during the synthesis of thymine nuclei, which is one of the main nitrogenous bases that constitute the DNA, , and without the nuclei thymine the DNA cannot multiply, thus cannot produce tumor growth (*10*).

Imiquimod is a compound also known as imidazoquinolones (*13*). It has the function of modifying the immune response in the body by stimulating the immune system to release cytokines due to the formation of an alpha-type interferon (IFN-α), as well as tumor necrosis factor-α (TNF-α) and, proinflammatory cytokines attributed to the heterocyclic structure. It also does not have stereoisomerism (*14* , *15*).

Imiquimod in contact with the skin activates macrophages, type B lymphocytes and Langerhans cells that cause the activation of the immune system in the lymph nodes (*15* , *16*). It is widely used in the treatment of skin cancer for the removal of superficial basal cell carcinoma (BCC) (*14* , *15*). It is also known for its excellent antiviral and antitumor activity (*13*). Imiquimod cream is used in actinic keratosis treatments, ie, flat, scaly growths on the skin caused by excessive exposure to UV rays on the face, scalp, neck, arms, hands, legs, and warts in the genital and anal areas.

Computational chemistry has allowed studying, understanding, and designing nanometric scale new controlled delivery systems for pharmaceutical applications.For example, the adsorption of drugs in chitosan

hydrogels has been studied to predict structural, chemical, and physical properties, FTIR, UV, and NMR at the nanometric scale (*8* , *17*). Computational chemistry consists of two principal areas: molecular or classical mechanics (MM) and quantum mechanics (QM). The analysis in MM requires the calculation of approximations primarily the Born–Oppenheimer.

In addition, Hooke's law is used as an approximation because the bonds between the atoms are a function of the harmonic potential as well as the transferability of the force field such as Assisted Model Building with Energy Refinement(AMBER), Chemistry at Harvard Macromolecular Mechanics (CHARMM), MM1, MM2, MM3 or MM4 (*18* , *19*). AMBER has also been designed with the purpose of studying pharmaceutical molecules. It allows for analysis in large areas of the conformational space with greater precision and lower computational cost as compared to Density Functional Theory (DFT) or Molecular Dynamic (MD) (*20* , *21*).

QM is widely used to study molecular interactions in new controlled release systems. QM performs the calculations from the nucleo-electron interactions because it is based on the Schrodinger's equation (*22*). Semi-empirical methods have the basis of calculation of Hartree-Fock (HF) in which the Hamiltonian and the wave function, respectively, are involved. It should be noted that a parameterization is established for the elimination of the calculation errors, which obtains data close to experimental results in the optimization geometry, dipole moments, reaction heats, ionization and electrostatic potentials and electronic spectra.

The parametrization method 3 (PM3) has a greater precision in the measurement of lengths and angles of bond is also efficient for the solvation reactions (*23*). The pharmaceutical industry has increased the modelling of a dataset by using quantum mechanics in the design of new controlled release systems to predict chemical properties, biological activity, toxicology, and pharmacokinetics and pharmacodynamics to analyze the release of drugs in hydrophilic matrices for the treatment of diseases (*24 – 25*). On the other hand the prediction of structural relations–biological activity (QSAR) in the pharmaceutical industry has represented an increase in the use of computational tools due to the information obtained as the molecular interactions, the biological behavior, structural properties, electrostatic and the distribution of charges for the design of the controlled release system.

The objective of this research was to determine the most stable molecular configuration in the adsorption process of the 5FU and imiquimod in chitosan hydrogels respectively, using the AMBER/PM3 hybrid model.

Materials and Methods

Geometry optimization

The calculation of the optimization geometry of 5FU, imiquimod, 5FU/hydrogel, and imiquimod/hydrogel was carried out on a DELL I5 computer. Using the HyperChem software, the AMBER model of molecular mechanics was firstly selected using the conjugate gradient method with a Polak–Ribiere algorithm and Root Mean Square (RMS) of 0.001 Kcal/Å–mol, respectively. Later, the calculation was performed using the PM3 model of quantum mechanics under the same conditions. The PM3 model allows for a better analysis of the hydrogen bonds and the effects attributed to the steric interactions. The purpose of this combination was to refine the molecular geometry, then to obtain an overall minimum in molecular geometry because the calculated heat of formation should be as negative as possible (*26*).

QSAR properties

HyperChem has the QSAR properties module in the Compute menu, where properties related to biological activity can be obtained. In controlled delivery systems, the partition coefficient parameter (Log P) shows the octanol/water ratio to determine whether the molecule is hydrophilic or hydrophobic in order to evaluate the similarity of the drug with a pharmacological or biological activity that could make it a possible active drug in the human body (*27* , *28*). Table 1 shows the ΔG (free energy of Gibbs) and the Log P of 5FU and the imiquimod calculated with the hybrid model AMBER/PM3 in which the negative negative value of the G indicates thermodynamic stability.

The Log P negative indicates that there is an affinity to the water contained in the hydrogel. On the other hand the positive value indicates that there are many factors affecting the adsorption like interaction forces between drugs and water that may involve electrostatic interactions, Van der Waals interactions, chemical affinity, and hydrogen bonds (*28* – *30*).

Table 1. 5FU and Imiquimod properties.

Properties	Units	5FU	Imiquimod
DG	Kcal/mol	- 43180.10	- 58905.50
Dipole moment	Debyes	3.570	4.522
Log P	----------	- 1.78	0.82

FTIR spectrum

From the Compute menu, the Vibration and rotation analysis option was selected and once the calculation was completed through the Compute–Vibrational spectrum option. The FTIR spectrum was selected and the vibrational mode was chosen by observing the different vibrational modes at several wavelengths (*26*). Table 2 shows the FTIR vibrations about 5FU in where, at3021 and 906cm^{-1}, were attributed to CH stretching vibrations, in the range between 1946–1901cm^{-1} and 331–124 cm^{-1}appeared band of carbonyl stretching (C=O). The peak at 1180 cm^{-1} belonged to C–F stretching band in the molecule of 5FU (*11* , *31* , *32*).

The FTIR vibrations of imiquimod structure are presented in Table 3 in where the CH stretching was observed at 3076–2871 cm^{-1}.The carbonyl stretching was localized at 1894–1647 cm^{-1} (strong and narrow).Finally, the C–C stretching was observed between 890–795 and 520–433 cm^{-1}.

Table 2. FTIR vibrations of 5FU by AMBER/PM3 hybrid model.

Bond	Vibration	Theoretical (cm^{-1})	Experimental (cm^{-1})
N-H	Stretching	3491, 3184, 789	3516, 3245, 3173
C-H	Stretching	3250-3168, 1015	3425, 3062
C=O	Stretching	1915-1876, 1715	1720, 1707
C=C	Stretching	1749	1743, 1649
C-N	Stretching	1564-1387, 1209-711	1650, 1580, 1038
C-F	Stretching	1214	1337, 1275, 1222
C-H	Stretching	1210	1243
C-F	Wagging	615-598, 459-311	804

Table 3. FTIR vibrations of imiquimod by AMBER/PM3 hybrid model.

Bond	Vibration	Theoretical (cm^{-1})	Experimental (cm-1) (36)
N-H	Symmetric stretching	3537-3429	3392
C-H	Asymmetric stretching	3076-2871	2960
C=O	Stretching	1894-1647	1668
C=C	Stretching	1782-1694	1531
C-C	Wagging	890-795, 520-433	960-875, 725-720
C-H	Wagging	795	730-710

Table 4 shows the vibrations of FTIR of the hydrogel (chitosan/genipin) where it is observed that the vibrations at 2320 and 1097 cm^{-1} were attributed to the cross-linking of the chitosan with genipin. The signal at 1097 cm^{-1} was assigned to the CN bond produced from the reaction of lysine with genipin, while the signal at 2320 cm-1 corresponded to the C-C, C-H, C-O, and C-N bonds obtained after cross-linking (*37* , *38*). The C=O stretching band of chitosan amide I at 1691 cm^{-1} was attributed to the cross-linking due to overlapping with C=C stretching with the genipin structure (*39*).

Table 4. FTIR vibrations of Hydrogel by AMBER/PM3 hybrid model.

Bond	Vibration	Theoretical (cm^{-1})	Experimental (cm^{-1})
OH and CH	Stretching	3676	3859, 3550
CH	Stretching	4901, 3885	3745
C=C	Stretching	3354, 1687	3398, 3245, 1630-1620
NH	Stretching	3314, 1545	3458, 3315, 3295, 1580
C-C, C-O	Stretching	2680, 2571, 1909, 1133, 489	2520, 1295, 1150, 793
CN	Stretching	1400, 1000	1360-1080
CC, CO, CH	Stretching	1445, 813	3089, 1440, 990, 721
C=O	Stretching	1691	1630

MESP (Molecular Electrostatic Potential)

Once the FTIR spectrum was obtained, the three–dimensional contour diagram with the electronic distribution of the molecule was obtained from the Compute menu and the plot molecular graphs option.

MESP was made with the objective of observing the nucleophilic and electrophilic zones, in addition to the distribution of the electron density of the HOMO and LUMO molecular orbitals (*40*). Figure 1 shows that the negative or electrophilic zones correspond to the C=O and C–F bonds in the 5FU as well as the C=N bond of the imiquimod, whereas the positive or nucleophilic zones are attributed to the NH and CH bonds, respectively.

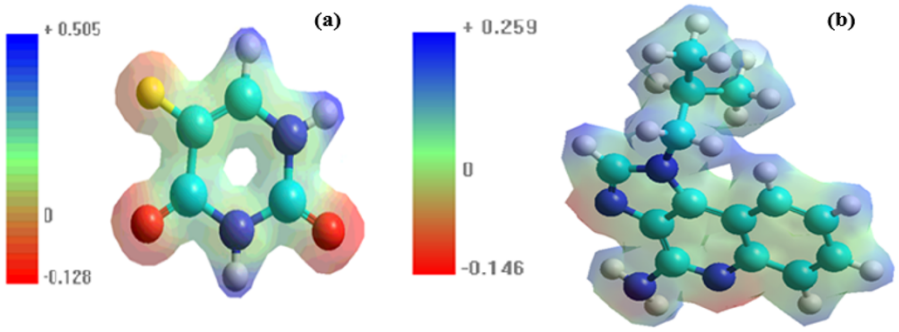

Figure 1. MESP of (a) 5FU and (b) Imiquimod by AMBER/PM3 hybrid model.

Results and Discussion

Structural properties

One of the objectives of the use of hydrogels in the design of new controlled release systems is to obtain a better vectorization and increase in the union of the soluble set with specific drugs (*41*). Table 5 shows Gibbs free energy (DG) which was calculated using the AMBER/PM3 hybrid model. This information allows analyzing the reaction mechanism for the formation of covalent bonds between the surface of the hydrogel and the drugs, allowing an increase on the affinity and maintaining the required pharmaceutical molecule size at the same time.Therefore, covalent drug interaction would increase the release of the biological effect.

A negative DG is also observed in both drugs indicating that the adsorption process is carried out spontaneously.

DG is attributed to the swelling of the chains of chitosan in the hydrogel due to the increase in volume during the adsorption, producing that the drugs to be diffused through the swollen hydrogel (*19*) due to the presence of sp^3 and sp^2 hybridizations responsible for the molecular recognition and stability of the drugs in both hydrogels as derivatives of the dispersion forces (*42*).

Table 5.Structural properties of the adsorption process of 5FU and Imiquimodin the hydrogel by AMBER/PM3 hybrid model.

Properties	Units	5FU/hydrogel	Imiquimod/ hydrogel
DG	Kcal/mol	- 22128.032	- 24459.301
Dipole moment	Debyes	5.121	8.193
Log P	---------	- 15.04	- 13.59

The change in the dipole moment (see Tables 1 and 5) is attributed to the electronegativity of the fluorine atom and C=N bond of 5FU and imiquimod, respectively. It indicates that there is an adsorption of the drugs on the surface of the hydrogel where there are Van der Waals forces or London dispersion forces (*43*). During the first stage, the adsorption mechanism is slow due to the barrier that generates the swelling affecting the diffusion of the drugs in addition to the covalent bonds responsible for the cross–linking of the hydrogels. It should be noted that the negative Log P indicates an increase in hydrophilic properties and electrostatic repulsion responsible for swelling of the hydrogel and subsequent adsorption of each drug (*44*). Although the fluorine atom causes low polarizabilities, it generates an increase in the hydrophilic capacity due to the rise of the dispersion forces in the hydrogel (*45*).

FTIR

Table 6 and Figure 2 show the main adsorption vibrations of 5FU in the hydrogel, in which the adsorption is verified by the displacements of the signals in the fingerprint region of the drug. The adsorption band characteristic at 1952 cm^{-1} 1 and 5. The C–H stretching is indicative of the adsorption process where the range of 3000 to 2728 cm was attributed to the symmetric C=O stretching.This band is very strong due to the change in the dipole moment as seen in Tables ^{3} hybridizations and above 3000 cm^{-1} corresponds to sp^{2} hybridizations. When approaching 3200 cm-1frequencies are assigned to the sp hybridization (*46*). The band at 1838 cm-1 is assigned to C=C stretching mode. Bands at 1457 cm^{-1} corresponded to N–H wagging, meanwhile the C–H wagging was observed at 1142 cm^{-1}, and the stretching C–F was observed at 1235–1189 cm^{-1}. Finally, fluorine atom in the hydrogel produces a displacement of the uracil ring from 795–789 to 778 cm^{-1} (*47*).

Table 6. FTIR vibrations of adsorption process of 5FU in the hydrogel by AMBER/PM3 hybrid model.

Bond	Wavelength(cm^{-1})	Vibration
O-H	3868-3836	Stretching (chitosan)
O-H	3764	Stretching (hydrogel/drug)
N-H	3528-3497	Symmetric stretching (chitosan)
N-H	3391	Asymmetric stretching (chitosan)
N-H	3324	Stretching (drug)
C-H	3127-2728	Stretching (hydrogel/drug)
C=O	1952	Symmetric stretching (drug)
C=O	1933-1919	Stretching (chitosan)
C=O	1919	Stretching (hydrogel)
C=C	1869, 1833	Stretching (genipin)
C=O	1860	Stretching (hydrogel/drug)
C=C	1838	Stretching (drug)
N-H	1457	Wagging (drug)
N-H	1667-1655	Scissoring (chitosan)
C-C	1460	Stretching (chitosan)
C-N	1379	Stretching (drug)
C-H	1142	Wagging (drug)
C-F	1235-1189	Stretching (C-F)
N-H, C-H	778	Wagging (hydrogel/drug)
N-H	639	Wagging (chitosan)
O-H	549	Wagging (chitosan)
C=O	523	Wagging (hydrogel/drug)
C=O	498	Wagging (drug)
O-H	439-176	Wagging (chitosan)
C-O	147-20	Wagging (chitosan)

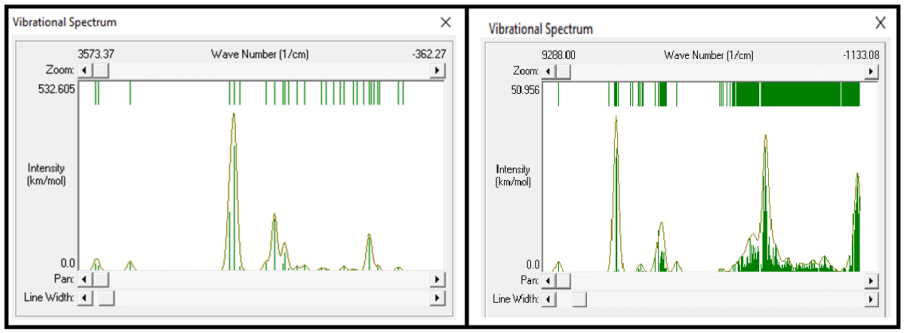

Figure 2. 5FU spectrum in where (a) before and (b) after the adsorption process in the hydrogel.

Table 7 and Figure 3 show that the adsorption of imiquimod is attributed to the formation of the hydrogen bond through the symmetrical and asymmetric stretching of the CH of the drug and the OH of the chitosan present in the hydrogel in the regions of 3893–3811 and 3792–3764 cm^{-1}. The bands between 2980 and 2965 cm^{-1} were assigned to the presence of C–H bonds (asymmetric and symmetric stretching). Those bonds were attributed to the presence of alkyl chain from the imiquimod on the surface of the hydrogel. The presence of the imiquimod amines was assigned in the 3586–3429 cm^{-1}. The amide I and II vibrations of the chitosan were observed at 3261, 1667–1661, 1533, 846, 808, 759, and 210 cm^{-1},however, there is the presence of an overlap at 1661 cm^{-1} attributed to the amides secondary effects of imiquimod. In addition, a shift in these bands is due to the formation of NH_2–NH_3^+ iterations of the water present in the hydrogel and the amines. The stretching of the O–H bond of the hydrogel was observed at 1564, 1467, 1400, 1367, 503–470, and 372–235 cm^{-1}, respectively (*48* , *49*).

Table 7. FTIR vibrations of adsorption process of Imiquimod in hydrogels by AMBER/PM3 hybrid model.

Bond	Wavelength (cm^{-1})	Vibration
O-H	3893-3811, 3792-3764	Stretching (hydrogel/drug)
N-H	3586-3429	Symmetric stretching (drug)
N-H	3261	Stretching (hydrogel)
C-H	3110, 2970	Stretching (hydrogel)
C-H	3042, 2916	Stretching (drug)
C-H	2980-2965	Stretching (hydrogel/drug)
C=C	1803-1695, 1558	Stretching (drug)
N-H	1667-1661, 210	Scissoring (chitosan)
N-H	1661	Scissoring (drug)
C=N	1602-1580, 1518	Stretching (drug)
C-N	1580, 1558, 1482, 1446, 1440	Stretching (drug)
O-H	1564, 1467, 1400, 1367, 503-470, 372-235	Wagging (hydrogel)
C-C	1558, 1006, 901 601	Wagging (drug)
N-H	1533, 808, 759	Wagging (chitosan)
C-C	1484-1482, 1423, 1271, 808	Stretching (genipin)
C-H	1250-1070	Stretching (glycoside ring)
C-N	901, 601	Wagging (drug)
N-H	846	Wagging (drug)

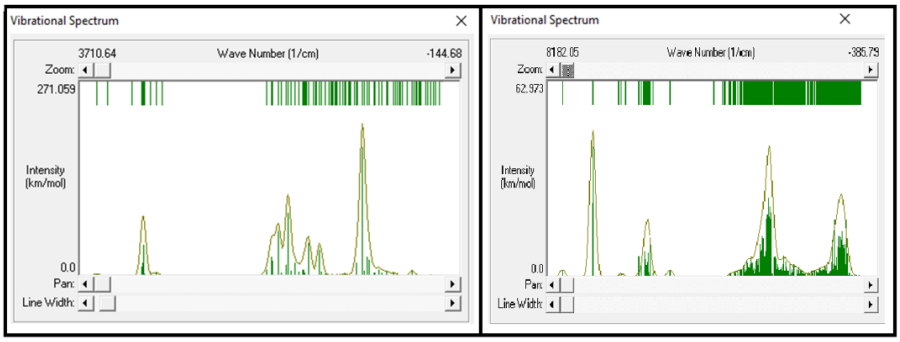

Figure 3. Imiquimod spectrum in where (a) before and (b) after the adsorption process in the hydrogel.

MESP

Figures 4a–5a show that the MESP attributed the local maxima corresponding to the electrophilic zones while the local minima were associated with the nucleophilic zones.The zones are defined through the zero–flow surface bounded by the saddle points (*50*). In addition, Figure 4a shows that the electrostatic distribution of the 5FU adsorption in the hydrogel had values ranging from 1.172 to -0.030 eV, where the electronegativity of the fluorine atom (yellow color) modifies the distribution of the electronic density that produces a decrease of electrons i.e. an oxidation (*51*) causing the formation of the hydrogen bridge bond at the surface of the hydrogel during the adsorption process (*52*). In pharmaceutical applications, the surface energy calculations observed in Figures 4b–5b are intended to determine the wettability and adhesion properties by the molecular interactions involved in the adsorption process such as cohesion, adhesion, mucoadhesion, and dispersion (*53*).The MESP of imiquimod adsorption is shown in Figure 5 where the electron distribution (0.988 to –0.025 eV) shows an increase in the nucleophilic zones due to the formation of hydrogen bonds during the adsorption as well as to electrostatic interactions and non–polar forces (*54*).

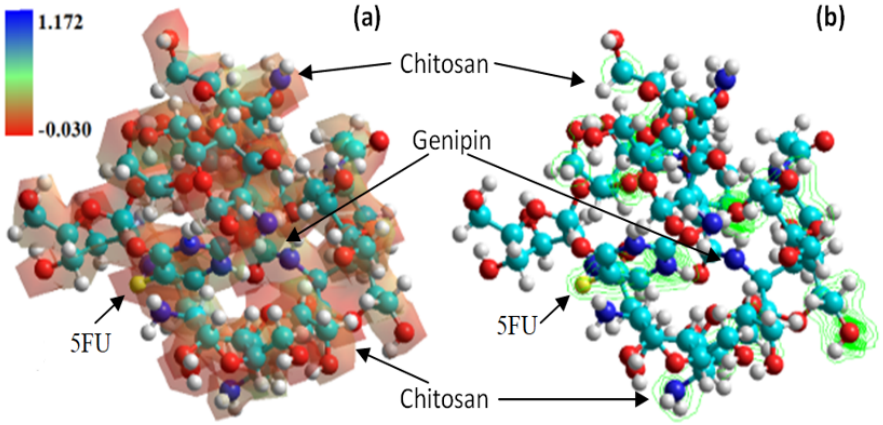

Figure 4. Maps of5 FU adsorption on chitosan hydrogel in where, (a) MESP and b) Surface energy respectively.

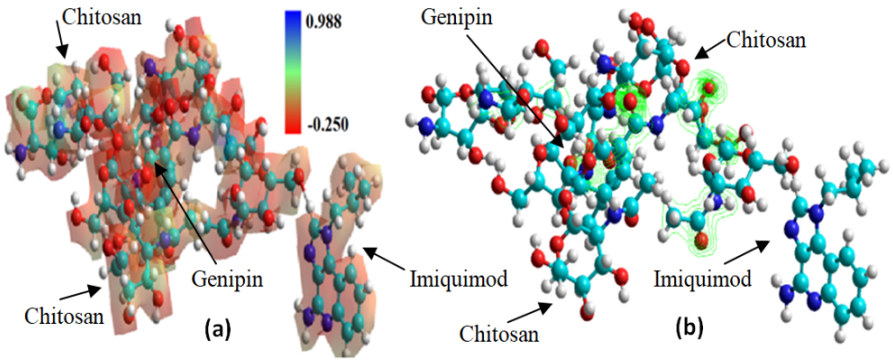

Figure 5. Maps of Imiquimod adsorption on chitosan hydrogel in where, (a) MESP and b) Surface energy respectively.

Conclusions

The AMBER/PM3 hybrid model of the molecular simulation allowed a complete analysis of the structure of the molecule through the identification of conformations of the hydrogel/drug adsorption. The Gibbs free energy determined that there is an adsorption of each drug and was verified because the greater the dipole moment, the greater the adsorption efficiency due to the electronegativity present in the drugs. FTIR showed the electronic distribution where the formation of hydrogen bonds between the hydrogel and the hydroxyl and amine groups of the drugs was observed. MESP showed that the difference seen in the values of the electronic distribution was attributed to the electronegative character of the bonds C-F, C=O and OH respectively.

References

1. Fortina, P.; Kricka, L. J.; Surrey, S.; Grodzinski, P. Nanobiotechnology: the promise and reality of new approaches to molecular recognition. TrendsBiotechnol. 2006, 23, 168-173. DOI: https://doi.org/10.1016/j.tibtech.2005.02.007.

2. Sáez, V.; Hernáez, E.; Sanz-Angulo, L. Sistemas de liberación controlada de medicamentos. Rev. Iberoamer. Polím. 2002, 3, 1-20.

3. Nuñez, R.;Jáuregui-Haza, U. J. Las nanopartículas como portadores de fármacos: características y perspectivas. Revista CENIC. 2012, 43.

4. Lohcharoenka, W.; Wang, L.; Chen, Y. C.; Rojanasakul, Y. Protein nanoparticles as drug delivery carriers for cancer therapy. BioMed Research International.2014, 2014, 1-12. DOI: https://doi.org/10.1155/2014/180549.

5. Orthaber, K.; Pristovnik, M.; Skok, K.; Peric, B.; Maver, U. Skin cancer and its treatment: novel treatment approaches with emphasis on nanotechnology. J. Nanomaterials. 2017, 2017, 1-20. DOI: https://doi.org/10.1155/2017/2606271.

6. Chen, J.; Shao, R.; Zhang, X. D.; Chen, C. Applications of nanotechnology for melanoma treatment, diagnosis, and theranostics. International Journal of Nanomedicine. 2013, 8, 2677–2688. DOI: https://doi.org/10.2147/IJN.S45429.

7. Ganji, F.; Vasheghani-Farahani, S.; Vasheghani-Farahani, E. Theoretical description of hydrogel swelling: A review. Iranian Polymer J. 2010, 19, 375-398.

8. Wang, D.; Green, MD.; Chen, K.; Daengngam, C.; Kotsuchibashi, Y. Stimuli-responsive polymers: Design, synthesis, characterization, and applications. International Journal of Polymer Science. 2016, 2016. DOI: https://doi.org/10.1155/2016/6480259.

9. Deepak, K.; Charak, S.; Mehrotra, R.; Kundu, S. FTIR and circular dichroism spectroscopic study of interaction of 5-fluorouracil with DNA. Journal of Photochemistry and Photobiology B: Biology. 2011, 105, 143–148. DOI: https://doi.org/10.1016/j.jphotobiol.2011.08.003.

10. http://www.cancerresearchuk.org/about-cancer/cancer-in-general/treatment/cancer-drugs/drugs/fluorouracil (Accessed, October 27th 2017).

11. Olukman, M.; Şanl, O.; Kondolot-Solak, E. Release of anticancer drug 5-Fluorouracil from different ionically crosslinked alginate beads. Journal of Biomaterials and Nanobiotechnology. 2012, 3, 469-479. DOI: https://doi.org/10.4236/jbnb.2012.34048.

12. Zhang, N.; Yin, Y.; Xu, S. J.; Chen, W. S. 5-Fluorouracil: Mechanisms of resistance and reversal strategies. Molecules. 2008, 13, 1551-1569. DOI: https://doi.org/10.3390/molecules13081551

13. Kumar, B. A. Imiquimod - Its role in the treatment of cutaneous malignancies.Indian J Pharmacol. 2015, 47, 354–359. DOI: https://doi.org/10.4103/0253-7613.161249

14. Pharmaceutical Benefits Branch. Aldara public summary document. PBAC meeting July 2006. http://www.health.gov.au/internet/wcms/publishing.nsf/Content/pbac-psd-imiquimod-july06 (Accessed, August 7th 2017).

15. Sauder, D. N. Imiquimod: Modes of action. British Journal of Dermatology. 2003, 149, 5–8. DOI: https://doi.org/10.1046/j.0366-077x.2003.05628.x

16. Schön, M.P; Schön, M. Imiquimod: Mode of action. British Journal of Dermatology. 2007, 157, 8–13. DOI: https://doi.org/10.1111/j.1365-2133.2007.08265.x

17. Martí, M. A. Simulación computacional de biomoléculas. un punto de encuentro entre la físico-química y la biología computacional. Anales Acad. Nac. de Cs. Ex., Fís. y Nat. 2013, 65, 43-49.

18. Favila-Pérez, MA. Actividad química teórica de fármacos contra mycobacterium tuberculosis favorecida por nanotubos y fullerenos. Ph.D. CIMAV, https://cimav.repositorioinstitucional.mx/jspui/bitstream/1004/223/1/Tesis%20Mar%C3%ADa%20Alejandra%20F%C3%A1vila%20P%C3%A9rez.pdf (Accessed, august 10th 2017).

19. Ferreira, LG.; Dos-Santos, R. N.; Oliva, G.; Andricopulo, A. D. Molecular docking and structure-based drug design strategies. Molecules. 2015, 20, 13384-13421. DOI: https://doi.org/10.3390/molecules200713384.

20. Stewart, J. J. P. Optimization of parameters for semi empirical methods IV: Extension of MNDO, AM1, and PM3 to more main group elements. J. Mol. Model.2004, 10, 155–164. DOI: https://doi.org/10.1007/s00894-004-0183-z.

21. Mendieta-Moreno, J. I.; Walker, R.; Lewis, J. P.; Gomez-Puertas, P.; Mendieta, J.; Ortega, J. FIREBALL/AMBER: An efficient local-orbital DFT QM/MM method for biomolecular systems. J. Chem. Theory Comput.2014, 10, 2185–2193. DOI: https://doi.org/10.1021/ct500033w.

22. Suarez, C.; Simulación con dinámica molecular de polímeros anfifílicos: dependencia del ph, longitud de la cadena polimérica y cadena alquílica. B.Sc. Universidad ICESI, 2013. https://repository.icesi.edu.co/biblioteca_digital/bitstream/10906/76492/1/simulacion_dinamica_molecular.pdf (Accessed, August 10th 2017).

23. Young, DC. (eds). Computational chemistry: A practical guide for applying techniques to real-world problems. WILEY, 2001. ISBN: 0-471-22065-5.

24. Parmar, NS.; Jethara, SI.; Patel, AD.; Patel, MR. A review literature and optimization of controlled drug delivery system using artificial neural network. JPSBR. 2015, 5, 306-314.

25. Mendyk, A.; Jachowicz, R.; Dorozynski, P. Artificial neural networks in the modeling of drugs release profiles from hydro dynamically balanced systems. Acta Poloniae Pharmaceutica Drug Research.2006, 63, 75-80. DOI: https://doi.org/10.1155/2015/863874.

26. http://chemistry.oregonstate.edu/courses/ch361-464/ch463/HYPERCH98.htm (Accessed, august 7th 2017).

27. Belaidi, S.; Mellaoui, M.; Electronic structure and physical-chemistry property relationship for oxazole derivatives by AB initio and DFT methods. Org. Chem. Int. 2011, 2011, 1-7.DOI: https://doi.org/10.1155/2011/254064.

28. Almi, Z., Belaidi, S.; Lanez, T.; Tchouar, N. Structure activity relationships, qsar modeling and drug-like calculations of tp inhibition of 1,3,4- oxadiazoline-2-thione derivatives. Int. Lett. Chem., Phys. Astron. 2014, 37, 113-124. DOI: https://doi.org/10.18052/www.scipress.com/ILCPA.37.113.

29. Bakkialakshmi, S.; Chandrakala, D. Thermodynamic studies on the interaction of 5-Fluorouracil with human serum albumin. Int. J. Pharm. Pharm. Sci. 2012, 5, 46-49. DOI: https://doi.org/10.1248/cpb.28.535.

30. Chao, K. P.; Lu, Y. T.; Yang, H. W. Prediction of partition coefficients of organic compounds between SPME/PDMS and aqueous solution. Int. J. Mol. Sci. 2014, 15, 2585–2595. DOI: https://doi.org/10.1016/j.aca.2015.09.010.

31. Yassin, A. E. B. ; Anwer, K.; Mowafy, H. A.; El-Bagory, I. M.; Bayomi, M. A.; Alsarra, I. A. Optimization of 5-fluorouracil solid-lipid nanoparticles: a preliminary study to treat colon cancer. Int. J. Med. Sci. 2010, 7, 398-408. DOI: https://doi.org/10.7150/ijms.7.398.

32. Bilensoy, E.; Curpanli, Y.; Sen, M.; Dogan, L.; Cahs, S. Thermosensitive muco adhesive gel formulation loaded with 5-Fu: cyclodextrin complex for HPV-induced cervical cancer. J. Incl. Phenom. Macrocycl. Chem. 2007, 57, 363-370. DOI: https://doi.org/10.1007/s10847-006-9259-y.

33. Garea, S. A.; Ghebaur, A.; Andronescu, C. Systems Based on Dendrimers and Antitumoral Drug Synthesized by Non-covalent Method the influence of dendrimers generation. Materiale Plastice. 2011, 48, 17-22.

34. Sunkara, S.; Sravanthi, D.; Maheswari, KM.; Salma, S.; Nallur, B. N. Development of modified release tablet dosage forms of capecitabine for better therapeutic efficacy. J. Chem. Pharm. Res. 2013, 5, 320-328.

35. Olukman, M.; Şanli, O.; Kondolot, E. Release of Anticancer Drug 5-Fluorouracil from Different Ionically Crosslinked Alginate Beads. J. Biomater. Nanobiotechnol. 2012, 3, 469-479. DOI: https://doi.org/10.4236/jbnb.2012.34048.

36. Dinesha.; Viveka, S.; Sandeep S. Laxmeshwar and GundibasappaKarikannarNagaraja. 1-{4-[(1-Isobutyl-1H-imidazo[4,5-c]quinolin- 4yl)amino]phenyl}ethanone. Molbank. 2012, M788; DOI: https://doi.org/10.3390/M788.

37. Klein, M. P.; Hackenhaar, C. R.; Lorenzoni, S. G.; Rodrigues, R. C.; Costa, T. M. H.; Ninow, J. L.; Hertz, P. F. Chitosan crosslinked with genipin as support matrix for application infood process: Support characterization and β-D-galactosidase immobilization. CarbohydratePolymers. 2016, 137, 184–190.DOI: https://doi.org/10.1016/j.carbpol.2015.10.069.

38. Dimida, S.; Barca, A.; Cancelli, N.; Grazia, R. M.; Demitri, C. Effects of Genipin Concentration on Cross-Linked Chitosan Scaffolds for Bone Tissue Engineering: Structural Characterization and Evidence of Biocompatibility Features. Int. J. Polym. Sci. 2017. DOI:https://doi.org/10.1155/2017/8410750.

39. Mirzaeil, E.; Faridi-Majidi, R.; Shokrgozar, M. A.; Asghari, P. F. Genipin cross-linked electrospun chitosan-based nanofibrous mat as tissue engineering scaffold. Nanomedicine J. 2014, 1, 137-146.

40. Rangel-Vázquez, N. A.; Rodríguez-Felix, F. Computational Chemistry Applied in the Analyses of Chitosan/Polyvinylpyrrolidone/Mimosa Tenuiflore (1st Ed.), 2013, Science Publishing Group Ed. Hong Kong.

41. Hamedani, S. Structural and electronic properties of folic acid adsorption on the carbon nanotubes: A density functional theory study. Orient. J. Chem. 2015, 31, 345-351. DOI:http://dx.doi.org/10.13005/ojc/310140

42. Stipdonk, M. J.; Badia-Martinez, D.; Sluijter, M.; Offringa, R.; Hall, T. V.; Achour, A. Design of agonistic altered peptides for the robust induction of ctl directed towards h-2db in complex with the melanoma-associated epitope gp100. Cancer Res. 2009, 69, 7784-7792. DOI: https://doi.org/10.1158/0008-5472.

43. Escobar, J. L.; García, D. M.; Zaldivar. D.: Katime, I. Hidrogeles. principales características en el diseño de sistemas de liberación controlada de fármacos. Rev. Iberoamer. Polím. 2002, 3, 1-25.

44. Rizwan, M.; Yahya, R.; Hassan, A.; Yar, M.; Azzahari, A. D.; Selvanathan, V.; Sonsudin, F.; Abouloula, C. N. pH sensitive hydrogels in drug delivery: Brief history, properties, swelling, and release mechanism, material selection and applications. Polymers. 2017, 9, 137; DOI: https://doi.org/10.3390/polym9040137.

45. Kirsch, P. Modern fluoroorganic chemistry: synthesis, reactivity, applications. Wiley-VCH, 2004.

46. http://www.ifsc.usp.br/~lavfis2/BancoApostilasImagens/ApLuminescencia/Infrared%20Spectroscop1.pdf (Accessed, August 13th 2017).

47. Farquharson, S.; Gift, A.; Shende, C.; Inscore, F.; Ordway, B.; Farquharson, C.; Murren, J. Surface-enhanced Raman spectral measurements of 5-Fluorouracil in saliva. Molecules. 2008, 13, 2608-2627. DOI: https://doi.org/10.3390/molecules13102608.

48. Pasqui, D.; Cagna, M.; Barbucci, R. Polysaccharide-Based Hydrogels: The key role of water in affecting mechanical properties. Polymers. 2012, 4, 1517-1534; DOI:https://doi.org/10.3390/polym4031517.

49. Kurecic, M.; Sfiligoj-Smole, M.; Stana-Kleinschek, K. UV polymerization of poly (n-isopropylacrylamide) hydrogel. Materials and technology. 2012, 46, 87–91.

50. Mata, I.; Espinosa, E.; Molins, E. Zero-flux surfaces of the electrostatic potential: The border of influence zones of nucleophilic and electrophilic sites in crystalline environment. J. Phys. Chem. A, 2007, 111, 9859–9870. DOI: https://doi.org/10.1021/jp074032l.

51. Kim, D.; Wang, L. et al. (2R)-4-Oxo-4-[3-(Trifluoromethyl)-5,6-dihydro[1,2,4]triazolo[4,3-a]pyrazin- 7(8H)-yl]-1-(2,4,5-trifluorophenyl)butan-2-amine: A Potent, Orally Active Dipeptidyl Peptidase IV Inhibitor for the Treatment of Type 2 Diabetes. J. Med. Chem., 2005, 48, 141–151. DOI: https://doi.org/10.1021/jm0493156.

52. http://adsabs.harvard.edu/abs/2015ApSS.359.474S (Accessed, august 13th 2017).

53. Fraser-Steele, D.; Moreton, R. C.; Staniforth, J. N.; Young, P. M.; Tobyn, M. J.; Edge, S. Surface Energy of Microcrystalline Cellulose Determined by Capillary Intrusion and Inverse Gas Chromatography. AAPS J. 2008, 10, 494–503. DOI: https://doi.org/10.1208/s12248-008-9057-0.

54. Zhang, R.; Somasundaran, P. Advances in adsorption of surfactants and their mixtures at solid/solution interfaces. Adv. Colloid Interface Sci. 2006, 123–126, 213–229. DOI: https://doi.org/10.1016/j.cis.2006.07.004.